International Journal of Technology 16(3) 933-948 (2025)

International Journal of Technology

http://ijtech.eng.ui.ac.id

Research Article

Artificial Intelligence-Based Optimal Design of Bi-directional Capacitor-Inductor-Inductor-Capacitor Converter for Electric Vehicle Applications

Rajalakshmi M [1], Razia Sultana Wahab [1,*]

[1] *School of Electrical Engineering, Vellore Institute of Technology, Vellore, 632014, Tamil Nadu, INDIA*
[*] *Corresponding author: wraziasultana@vit.ac.in; Tel.: +9104162202362*

Abstract: Artificial intelligence (AI) based converter design is a model that greatly reduces the complexity of manual calculations, accelerates the design process with reduced loss, and achieves high efficiency. The optimized design significantly decreases the cost due to its high power density and reduced component size. Moreover, Capacitor-Inductor-Inductor-Capacitor (C2LC) DC-DC resonant converter for Electric Vehicle (EV) charging designed with high frequency includes complex electromagnetic design of resonant tank parameters. There may be a chance of inaccuracy in the design parameters due to the manual intervention and complex design parameters. Therefore, this study focused on the optimal design of C2LC converter by using Hybrid Teaching-learning-Based Optimization (TLBO)+Particle Swarm Optimization (PSO) algorithm for minimized total power loss and accurate magnetic core design to operate the converter at maximum efficiency. The optimization reduced the computational complexity of the converter design and total losses. Finally, a 48V EV charger was implemented, and the results were explored. During the process, the efficiency of C2LC converter with conventional design and the proposed hybrid TLBO+PSO optimized design was compared. About 1% efficiency was higher for the optimized design of the converter than the other for various load conditions.

Keywords: AI-based EV charger; Hybrid teaching-learning-based optimization; Resonant converter

1. Introduction

Power converters play a crucial role in power transmission systems, enabling the transformation of voltage and current to different levels based on load requirements (Jamahori et al., 2024). The demand for bi-directional DC-DC power converters is rapidly increasing in applications such as energy storage systems (Attia and Suan, 2024), wireless charging (Jayalath and Khan, 2021), solid-state transformers (Li et al., 2023), and DC grids. Among these, Dual Active Bridge (DAB) converters are widely used for bi-directional operation capability and the ability to handle high power at high operating frequencies (Mirtchev and Tatakis, 2022). Transformers require a higher number of secondary turns for low-voltage applications, which leads to increased parasitic inductances and capacitances. These parasitic elements negatively impact converter performance by increasing power losses (Shalbaf et al., 2024). LC resonant-based DAB converters are used to address the issue of hard switching in DAB converters, offering improved performance under narrow input voltage variations and limited frequency control bandwidth (Liu et al., 2022). For applications requiring wide voltage and frequency control bandwidth, Capacitor-Inductor-Inductor-Capacitor (C2LC) converter provides a solution. The converter features an LC tank on

This work was supported by the 'Vellore Institute of Technology' funded by Royal Academy of Engineering, Award reference No. TSP-2325-5-IN\172

https://doi.org/10.14716/ijtech.v16i3.7486
Received November 2024; Revised December 2024; Accepted March 2025

both the primary and secondary sides of high-frequency transformer (HFT), improving efficiency as well as control flexibility (He and Khaligh, 2017). Furthermore, the optimized design of the transformer combined with a unified control strategy significantly improves the total performance of the converter (Rajalakshmi and Sultana 2023; Lee et al., 2021).

Various modifications have been performed on the resonant tank section to meet specific application requirements (Zhou et al., 2022). Recently, reconfigurable structures have been introduced to enable broad voltage regulation (Nagesha and Lakshminarasamma, 2023). A main challenge in C2LC converter is the optimal selection of LC values to achieve soft switching under varying load conditions (Mukherjee and Barbosa, 2023). To address this, a unified design model has been proposed to reduce the complexity of parameter selection and ensure smooth synchronous rectification (SR) (Rajalakshmi and Sultana, 2024). Achieving natural SR relies heavily on the proper selection of LC resonant tank values, which play a crucial role in minimizing switching transition losses (Rajalakshmi and Sultana, 2022). A hybrid control strategy combining dual phase-shift and duty cycle control has been proposed to further improve the efficiency of C2LC converter, though this method adds implementation complexity (Rajalakshmi et al., 2021). Despite incorporating AI methods into power converter control which can significantly improve performance, the design process still requires careful attention to minimize both cost and power losses (Hajihosseini et al., 2020). Moreover, the design of incorporated high-frequency transformers (HFTs) for cost reduction and precise measurement of leakage inductance adds further complexity to the total system design (Ansari et al., 2022).

The design of converters is typically performed in two phases, namely (1) mathematical derivation and analysis of converter parameter objectives as well as constraints, and (2) evaluation of optimized circuit parameters using iterative methods (Hasanah et al., 2024). Traditionally, these two steps have been performed manually, a process categorized as Human-Dependent Approach (HDA). Computer-Aided Approach (CAA) was later introduced to assist in evaluating optimized circuit parameters. However, the traditional design method is prone to errors due to assumptions made during analysis and is often difficult because of complex mathematical expressions (Lee et al., 2019). CAA helps reduce this burden by using optimization algorithms for parameter evaluation (Hannan et al., 2020). In recent years, the incorporation of Artificial Intelligence (AI) for the optimization of both design and controller parameters has significantly improved the accuracy and performance of converters modified to specific applications (Lin et al., 2024). The incorporation of AI has further simplified the design process by fully automating both phases, leading to what is now known as Automatic Artificial Intelligence Approach (AAIA).

The use of optimization algorithms is rapidly increasing across various fields to reduce manual intervention and improve performance through optimal design. In the context of power converters, metaheuristic algorithms have surfaced as viable alternatives for addressing large and complex optimization problems related to design, control, and operation (De Leon-Aldaco et al., 2015). Several well-established algorithms such as Genetic Algorithm (GA) (Yashin *et al.*, 2020; Binay Kumar *et al.*, 2018), Particle Swarm Optimization (PSO), Ant Colony Optimization (ACO), and Artificial Immune System (AIS), have been widely implemented due to the robustness, simplicity, universality, as well as single-solution search capabilities (Dharma and Setiawan, 2024; Jayawardana et al., 2019). Following the discussion, the convergence speed of these optimization algorithms often depends on the selection of initial parameter values (Mao et al., 2024). In specific applications, such as tuning the parameters of fractional-order PID controllers for buck converters, Fitness-Distance Balance-Based Runge-Kutta algorithm has been effectively used (Isen, 2022). For motor design optimization, Extreme Learning Machine (ELM) algorithm has also been successfully implemented (Song et al., 2019).

In Lin et al. (2024), a combination of Support Vector Machine (SVM), Extreme Gradient Boosting (XGBoost), and Differential Evolution was used to optimize DAB converter design by developing an accurate current stress model. Optimal efficiency was achieved through the incorporation of XGBoost and PSO with a State-Based Adaptive Velocity Limit algorithm for extended phase-shift control (Li et al., 2023). Moreover, the Soft Actor-Critic method that was based on Deep Reinforcement Learning, has been used to optimally tune the nonlinear controller of a full-bridge converter (Fathollahi et al., 2023). An autonomous topology generator using a reinforcement learning framework was proposed to design power converters with minimized cost and size, while maximizing efficiency and reliability (Silva et al., 2023). PSO has been widely recognized for its fast convergence speed, simplicity, and high accuracy (Rahman et al., 2016). However, the performance of the model can be limited by the premature convergence problem (Priyadarshi et al., 2019). To address the issue, Teaching-Learning-Based Optimization (TLBO) algorithm has acquired attention for its effectiveness in a variety of scientific and engineering applications (Zhou et al., 2023). TLBO operates in two iterative phases, namely teaching and learning—to achieve maximum accuracy in parameter optimization (Khorashadizade and Hosseini, 2023). The algorithm has also been applied to improve the performance of PSO by extracting optimized convergence parameters, effectively overcoming PSO's premature convergence issue.

The hybrid TLBO+PSO optimisation is proposed in this study to overcome the challenges of C2LC converter design from the literature survey. The analysis is structured into Section II, which describes the challenges in the existing design method of C2LC converter for Electric Vehicle (EV) charger. The section also explains the derivation of C2LC circuit main parameters, with modes of operation, Zero Voltage Switching (ZVS) constraints, and total power loss equation calculation. Additionally, Section III explains the detailed process of AAIA-based C2LC converter design using a hybrid TLBO+PSO algorithm and electromagnetic analysis for optimal design of HFT parameters. Section IV shows the simulation and experimental results for AAIA-based design values of the converter, and the conclusion is written in Section V.

2. Challenges in Existing Design Method and Proposed Solution

2.1. Challenges in Existing Conventional Design Process

Figure 1 showed the block diagram of the application of a C2LC converter for an EV charger. C2LC resonant converters were able to handle a wide range of load voltages, as well as better regulation and reaction to load fluctuations were made possible by the resonant functioning. These converters were suited for applications with dynamic load profiles because the models maintained good efficiency and voltage regulation over a wide range of loads. The main issues to be considered were the assigned and selected parameters, as the voltage gain was known to be a function of frequency ratio, load values, and inductance ratio, which had to be carefully selected for better converter performance. Another issue in a C2LC converter is related to holding the input voltage bus constant without affecting the resonant waveforms.

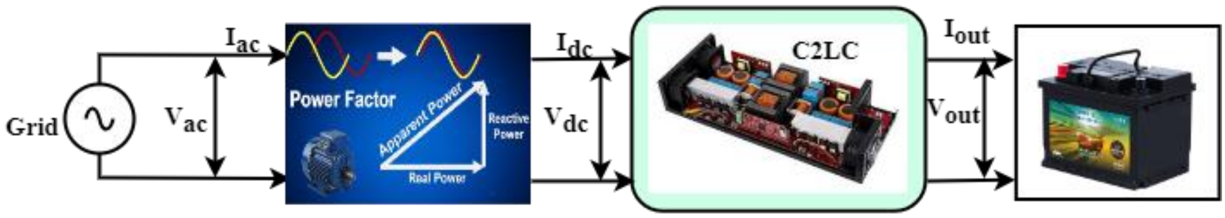

Figure 1 Role of C2LC converter in EV charging

The bi-directional C2LC converter design procedure included two significant essential steps. The first step was the mathematical derivation as well as analysis of converter parameter objectives and constraints to obtain an accurate model of the converter. In the second step, using the model derived from the first step, the circuit parameters were optimized based on the defined constraints. Traditionally, these two steps were conducted through manual intervention, which was a very tedious process due to the complexity of the mathematical analysis and the iterative process required to arrive at the optimized parameter values. The accurate model of the converter in HDA was not easily obtained due to the many assumptions in the study, leading to inaccurate circuit parameter values. Relating to the process, the human trial-and-error iterative method was timeconsuming in the optimization step, and there was no guarantee of accurately obtaining the optimized value.

The great development of optimization algorithms simplified the iterative process previously performed by human intervention, reduced the burden on humans, and increased the accuracy of circuit parameter optimization. This CAA dramatically reduced computational time with the help of optimization algorithms and was very suitable for multi-objective parameter optimization. Despite the assistance of CAA in the iterative process, the mathematical analysis as well as the deduction process limited its application and was highly complicated due to the many assumptions in the analysis. CAA became precise when mathematical analysis produced more accurate and consistent results. Additionally, the optimization algorithm was performed based on manual calculations, which needed to be error-free. The optimization algorithm provided the most accurate result, building on the precise mathematical evaluation conducted earlier.

2.2. TLBO-PSO Automated Parameter Optimization

During this study, the parameters of C2LC resonant converter, transformer leakage inductances of the primary and secondary sides, magnetizing inductance, as well as primary and secondary capacitances were optimized using TLBO+PSO algorithm. TLBO was a meta-heuristic algorithm that optimized the objective function based on the population present in the classroom environment. In the classroom, the teacher worked hard to educate all the students. Moreover, the learners then communicated with each other to change and improve the acquired knowledge. The process included two phases, namely Teacher and Learner phase. In Teacher phase, the students learned from teacher and acquired knowledge. In Learner phase, the students improved the knowledge by interacting with each other, as shown in Figure 2.

Figure 2 Flowchart of TLBO algorithm

2.3. Circuit Analysis of C2LC Converter.

The circuit diagram of the open-loop control C2LC resonant converter for a battery charging application was shown in Figure 3(a). The image included front-end inverter (Q_1, Q_2, Q_3, and Q_4), isolated by HFT, with an LC resonant tank on both the primary and secondary sides, and followed by rectifier stage (Q_5, Q_6, Q_7, and Q_8). During the process, 50% duty cycle square wave was used to achieve higher efficiency irrespective of the sinusoidal input voltage. The resonance property enabled the resonant tank circuit to offer lower impedance to the sinusoidal current at the resonant frequency. In the analysis, switching frequency (f_s) relative to resonant frequency (f_r) determined the performance of the converter.

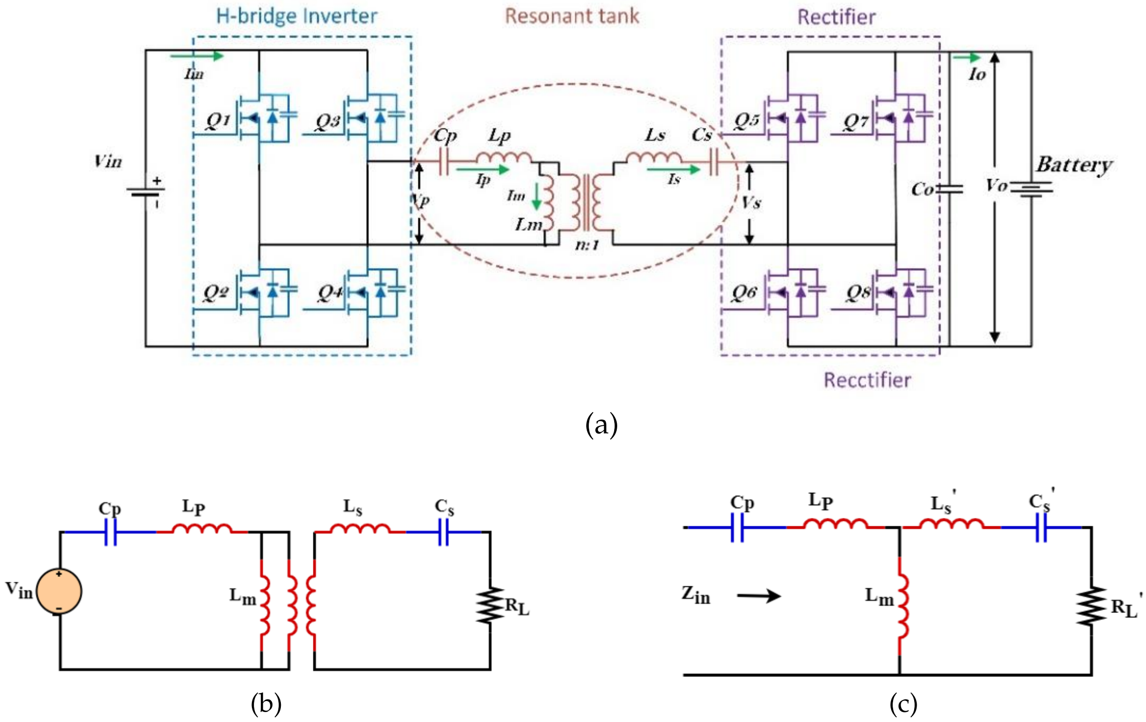

Figure 3(a) Circuit diagram of C2LC converter, (b) Equivalent circuit of C2LC converter, (c) Input impedance with referred to primary

The equivalent circuit to derive the impedances was shown in Figure 3(b) and (c)(Martins et al., 2019). The primary and secondary leakage inductances and capacitances were L_p, L_s, as well as C_p, C_s, and the magnetization inductance L_m with turned ratio n:1. Moreover, R_L was the secondary side load of the converter, L_s', C_s', and R_L', were the secondary side parameters referred to as the primary side. Equations (1-4) showed the derivation of primary side impedance (Z_p), secondary side impedance referred to primary (Z_s'), and magnetizing impedance (Z_m) from the load resistance referred to primary (R_L').

$$Z_p = \frac{1}{j\omega_s C_p} + j\omega_s L_p \tag{1}$$

$$Z_m = j\omega_s L_m \tag{2}$$

$$Z_s' = \frac{1}{j\omega_s C_s'} + j\omega_s L_s' \tag{3}$$

$$R_L' = \frac{8n^2}{\pi^2} R_L = \frac{8n^2 V_o^2}{\pi^2 P} \tag{4}$$

Secondary side resonant parameters with referred to primary was derived from

$$\mathrm{L_s' = n^2 L_s, C_s' = \frac{C_s}{n^2}} \tag{5}$$

The input impedance was calculated by

$$\mathrm{Z_{in} = Z_p + Z_m \parallel (Z_s' + R_e')} \tag{6}$$

$$\mathrm{I_{p,rms} = \frac{V_{in}}{\sqrt{2}Z_{in}}\ , I_{s,rms} = \frac{nV_o}{\sqrt{2}Z_o}} \tag{7}$$

The symmetrical peak magnetizing current $I_{m,p}$ under a steady state was calculated by

$$\mathbf{I_{m,p} = \frac{V_{in}T_s}{4L_m}} \tag{8}$$

To calculate the core loss of the transformer, the peak magnetic flux density B_p was evaluated by

$$B_p = \frac{L_m I_{m,p}}{n_p A_m} \tag{9}$$

Where T_s was the switching period, n_p represented the number of primary winding turns, and A_m signified the magnetic core cross-sectional area. The voltage gain equation for C2LC converter derived from the equations previous was,

$$\boldsymbol{G = \frac{V_o}{V_{in}} = \frac{[Z_m \parallel (Z_s' + R_L')]\, R_L'}{[Z_p + [Z_m \parallel (Z_s' + R_L')]](Z_s' + R_L')n}} \tag{10}$$

2.4. Constraints for ZVS and Power Loss Equations

Small dead time (T_d) was introduced between each transition to prevent cross-conduction and to give sufficient time for the complete discharge of the switches output capacitance (C_{oss}) in achieving ZVS. During the analysis, the condition for ZVS was,

$$\boldsymbol{T_d \geq 16 C_{oss} f_s L_m} \tag{11}$$

The soft commutation was achieved by reserving the condition, $f_s \leq f_r$. Despite the reduction by ZVS in the switching losses, the total power losses(P_t) due to conduction loss (P_c=P_{I_c} + P_{R_c}) and switching loss (P_S=P_{I_s}+P_{R_s}) of both inverter as well as rectifier stages were significant in performance for designing the converter with high efficiency. Additionally, driving loss of both inverter and rectifier (P_d=P_{I_d}+P_{R_d}) of the switches, power loss of resonant capacitance (P_{Cr}) copper loss (P_{cu}), as well as core loss (PFe) of the transformer, was also significant in performance for designing the converter which was derived by,

$$P_t = P_d + P_s + P_c + P_{cu} + P_{Fe} + P_{Cr} \tag{12}$$

- Driving loss of the switches:

$$P_d = P_{I\_d} + P_{R\_d} = 4(Q_{I_g} V_{I_{gs}} f_s + Q_{R_g} V_{R_{gs}} f_s) \tag{13}$$

- Switching loss of the Inverter and rectifier:

$$\boldsymbol{P_s = P_{I\_s} + P_{R\_s} = (n^2 + 1)(I_{m\_p}^2 T_d^2 f_s)/(12 C_{oss})} \tag{14}$$

- Conduction loss:

$$\boldsymbol{P_c = P_{I\_c} + P_{R\_c} = 2(I_{p,rms}^2 R_{I_{on}} + I_{s,rms}^2 R_{R_{on}})} \tag{15}$$

- Transformer Copper loss:

$$\boldsymbol{P_{cu} = I_{p,rms}^2 R_T + I_{s,rms}^2 R_T} \tag{16}$$

- Transformer core loss:

$$\boldsymbol{P_{Fe} = k_c f_s^{\alpha} B_p^{\beta} V_c} \tag{17}$$

- Resonant capacitances power loss:

$$P_{Cr} = \frac{I_{p,rms}^2 tan\theta}{2\pi f_s C_p} + \frac{I_{s,rms}^2 tan\theta}{2\pi f_s C_s} \tag{18}$$

3. Proposed AAIA for The Design of The Converter

AAIA was proposed to automate the two phases of the design steps of the converter to handle all the difficulties of converter design parameters. Figure 4 showed an understanding of the manual, semi-optimized converter design process that was fully automated. During the process, the evaluation of optimized circuit parameters by iterative method was conducted using hybrid TLBO+PSO algorithm. This study aimed to optimize total power loss, including switching, conduction, resonant capacitance, copper, and transformer core losses. An optimal design method was proposed using TLBO+PSO algorithm. Moreover, the main parameters were optimized for minimum losses, and HFT optimal leakage and magnetic inductances were obtained based on hybrid electromagnetic analysis.

Steps for converter design	*HDA*	*CAA*	*AAIA*
Mathematical derivation and analysis of converter parameter objectives and constraints	Manual intervention	Manual intervention	AI-tool
Evaluation of optimized circuit parameters by iterative method	Manual intervention	Metaheuristic algorithms	Metaheuristic algorithms

Figure 4 Understanding of converter design process of manual, semi optimized and fully automated

The inaccurate HAD design was rectified by CAA design, and then the remaining inaccuracy problem was addressed with the help of an AI tool to fully automate the design process of C2LC converter. This AAIA facilitated accurate design parameters and easy implementation after the converter design process. The combination of AI tool models and optimization algorithms made the design processes of various applications simple and boundless.

3.1. AAIA-based design of C2LC converter

AAIA-based open-loop C2LC resonant DC converter was detailed in this section for the optimized total power loss, as per the equations derived in the previous Section 2.5. Two stages were included in optimizing the method for C2LC converter design. In the first stage, the resonant tank parameters were optimized. Additionally, the high-frequency planar transformer leakage inductances and magnetizing inductances were designed using hybrid electromagnetic analysis in the second stage. The proposed TLBO+PSO and PSO algorithm flowchart for the optimized design were shown in Figure 5(a) and (b).

3.1.1. Stage 1: Parameter optimization based on total power loss (TLBO+PSO)

- Objective: To find the resonant tank parameters of C2LC converter L_{r1}, C_{r1}, L_{r2}, C_{r2}, and L_m for the optimized minimum total power loss.

During this stage, the total power loss of C2LC converter was optimized using a hybrid AI algorithm. The primary issue with PSO was the need for a high iteration count to achieve global optimum value. Moreover, the manual initialization of the parameters compromised the iteration count to get the desired accuracy. The four main factors that decided PSO algorithm efficiency were Wt.st (weight start), Wt.ed (weight end), Kd(kind), and Vel.max (velocity maximum). The optimized selection of these parameters increased the convergence speed. This problem could be solved by hybrid algorithm TLBO+PSO to optimize the parameters Wt.st, Wt.ed, Kd, and Vel.max in decreasing the iteration count and causing reduced computational time.

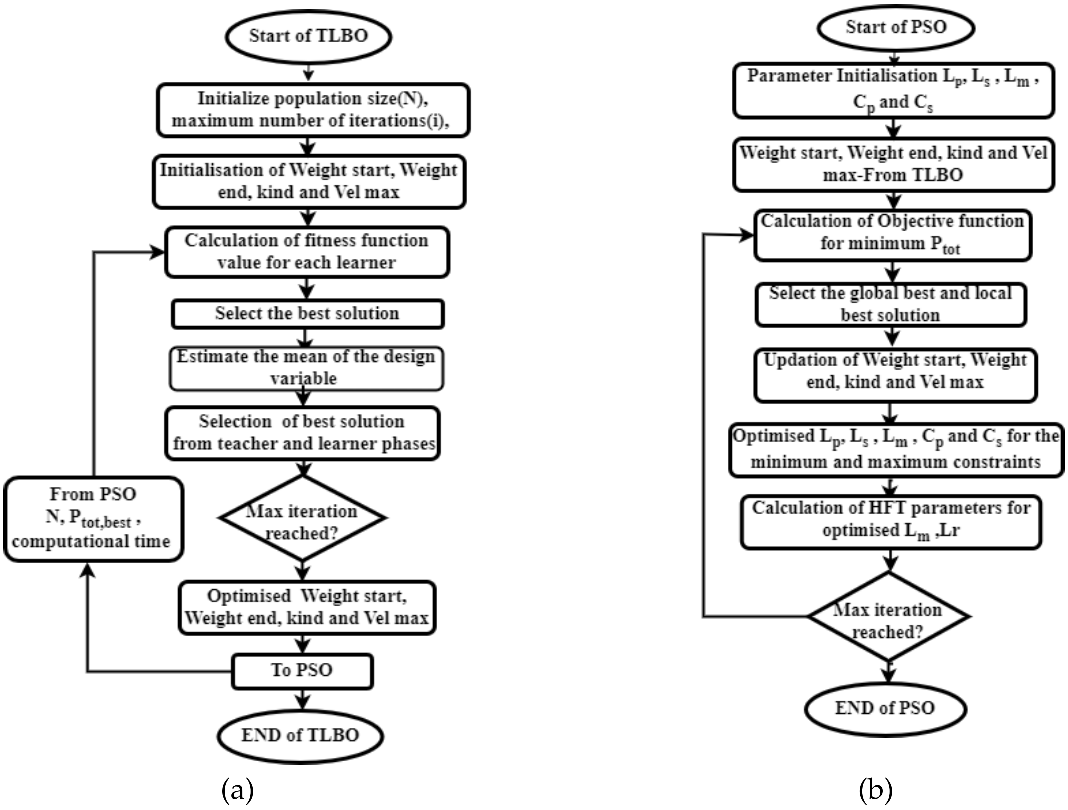

Figure 5 (a) Flowchart of the proposed TLBO+PSO algorithm, (b) Flowchart of the PSO algorithm

The improvised PSO algorithm of TLBO optimized the system, which started from TLBO algorithm where the best student of each parameter (Wt.st, Wt.ed, Kd, and Vel.max) was sent to the algorithm. The optimized value of the number of iterations (N) and the total power loss (P_{tot}) of PSO was obtained with these optimized parameters from TLBO algorithm. Relating to the process, this value was sent back to TLBO to find the fitness value. Repeatedly, the parameter value was optimized, and feedback was given to PSO. This process was iterated to obtain the optimized value of those four parameters of PSO up to maximum iteration of TLBO. The optimized values of L_p, L_s, L_m, C_p, and C_s were found for the minimum total power loss value with those optimized parameters. The steps included in hybrid TLBO+PSO algorithm were described in the following steps.

Step 1: Initialisation of TLBO algorithm parameters population size(N), maximum number of iterations, TF was the teaching factor which could be 1 or 2, Rand represented the random number of lies between 0 to 1. The TLBO algorithm optimized Wt.st, Wt.ed, Kd, and Vel.max of PSO algorithm by finding the best student for each parameter through simulating both the teaching as well as learners phase.

Step 2: Stimulation of PSO algorithm to find the maximum number of iterations and optimized P_{tot} for the optimized Wt.st, Wt.ed, Kd, and Vel.max from TLBO. After the execution of PSO, N and P_{tot} were found, the models were used to evaluate the fitness value of TLBO. The optimized P_{tot} value was ensured to be in the limit based on the constraints to achieve maximum efficiency.

Step 3: The optimized N and P_{tot} from PSO were feedback to TLBO algorithm to evaluate the fitness value. This process was repeated until the maximum iteration of TLBO algorithm was reached. Finally, the optimized L_p, L_s, L_m, C_p, and C_s were found for the optimized $P_{tot.}$

The optimized values of L_p, L_s, L_m, C_p, and C_s were evaluated for the given power, frequency, and voltage gain concerning the values shown in Table 1. The total power loss (P_{tot}) results for each iteration of the proposed TLBO+PSO algorithm were compared with PSO, GA, ACO, and BCO (Bee colony optimization) for proving the best algorithm in Figure 6. The process showed the hybrid

TLBO+PSO algorithm which provided best design parameter values for the lowest P_{tot} with less iteration count. Additionally, the iteration count for optimum P_{tot} was shown in Table 2, proved that the hybrid TLBO+PSO algorithm indicated better performance compared to the other algorithms.

Table 1 Parameters of C2LC converter

Parameter	Value	Parameter	Value
Input grid voltage	230V	L_p	42.12µH
Output voltage	48V	L_s,	32.4µH
Power	3kW	L_m	337 µH
Switching frequency	85kHz	C_p,	83.3nF
Resonant frequency	85kkHz	C_s	108.3nF

Table 2 Power loss and iteration count of algorithms

Algorithm	Iteration number	Total power loss (W)
PSO	82	18.6
GA	65	19.3
ACO	58	18.3
BCO	69	18.5
TLBO+PSO	33	17.8

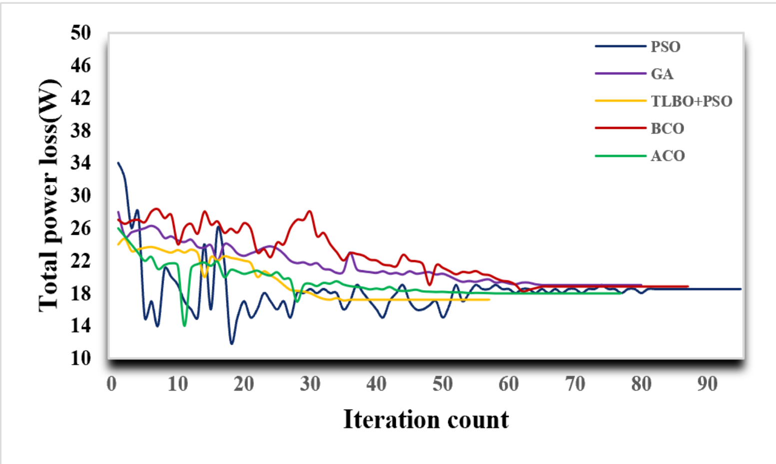

Figure 6 Optimised power loss for PSO, GA, BCO, ACO, Proposed

3.1.2. Stage 2: Hybrid Electromagnetic Analysis for Designing HFT Parameters (Li et al., 2022)

- Objective: To optimize the Leakage inductances and magnetizing inductances of HFT based on winding dimensions as well as air gap between primary and secondary winding.
  - ❖ Leakage inductance optimization

The leakage inductances of the transformer (L_{r1}& L_{r2}) were used as the resonant tank inductances to increase the power density of the power converters, which reduced the volume and weight of the converter by reducing the number of magnetic components. The transformer winding and insulation dimensions, as well as the distance between the primary and secondary winding, were used to optimize the leakage inductances of HFT. Moreover, the insulation thickness (d_i), primary and secondary winding thickness (d_p &d_s), as well as winding distance (l_b) were derived to achieve the desired leakage inductances. Figure 7(a) showed the winding configuration of the high-frequency planar transformer and its magneto-motive force (MMF). The primary winding was distributed over m_p layered with n_p number of turns. Additionally, the secondary winding was distributed over m_s layered with n_s number of turns. The magnetizing inductance was optimized by including the aig gap parameter (l_g). For the current excitation of I_p in the primary winding, the magnetic energy was calculated based on MMF distribution by Eq (19).

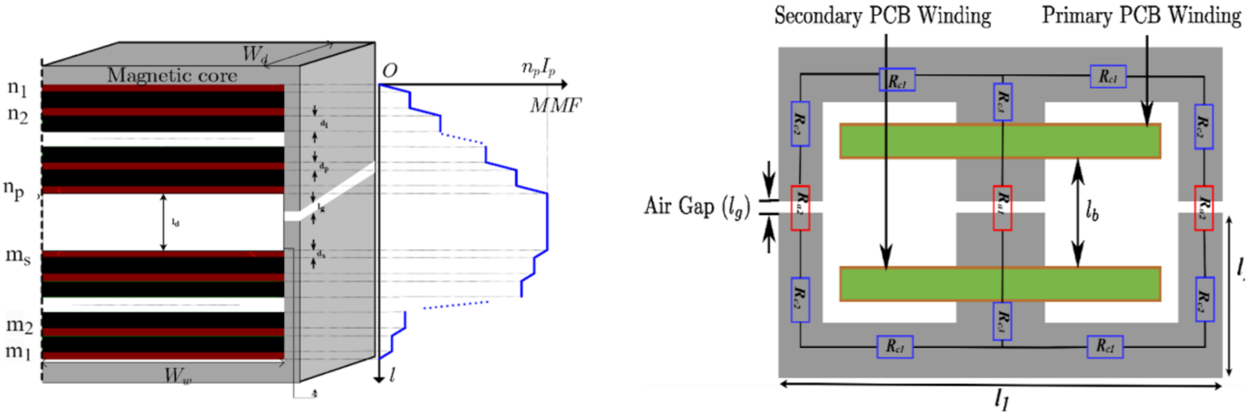

(a) (b)

Figure 7(a) Winding configuration of HFT (b) 3D model of HFT equivalent magnetic circuit with airgap

$$\mathbf{E_m} = \frac{\mu_0\mu_r n_p^2 I_p^2 W_d}{6W_w}\left[2m_pd_p + 2m_sd_s + \frac{(m_p-1)(2m_p-1)}{m_p}d_i + \frac{(m_s-1)(2m_s-1)}{m_s}d_i + 6l_b\right] \quad (19)$$

Where W_d & W_w were the depth and the width of the window. From the magnetic energy equation, the leakage inductances were calculated by

$$L_{lp} = L_{ls} = \frac{E_m}{I_p^2} = \frac{\mu_0\mu_r n_p^2 W_d}{6W_w}\left[2m_pd_p + 2m_sd_s + \frac{(m_p-1)(2m_p-1)}{m_p}d_i + \frac{(m_s-1)(2m_s-1)}{m_s}d_i + 6l_b\right] \quad (20)$$

From the previous equation, l_b could be arrived for the leakage inductance value obtained from the optimization,

$$l_b = \frac{W_wL_{lp}}{\mu_0\mu_r n_p^2 W_d} - \frac{m_pd_p}{3} - \frac{m_sd_s}{3} - \frac{(m_p-1)(2m_p-1)}{6m_p}d_i - \frac{(m_s-1)(2m_s-1)}{6m_s}d_i \quad (21)$$

❖ Magnetizing inductance optimization

The magnetizing inductance was optimized by adjusting the thickness of the airgap (l_g). Figure 7(b) showed the 3D model of HFT equivalent magnetic circuit. In addition, the calculation of magnetic reluctances R_{c1}, R_{c2}, R_{c3}, R_{a1}, and R_{a2} were evaluated by,

$$R_{c1} = \frac{l_1}{\mu_0\mu_r A_e} \quad (22\text{-}1)$$

$$R_{c2} = \frac{2l_2}{\mu_0\mu_r A_e} \quad (22\text{-}2)$$

$$R_{c3} = \frac{2l_2}{\mu_0\mu_r A_e} \quad (22\text{-}3)$$

$$R_{g1} = \frac{l_g}{\mu_0 A_e} \quad (22\text{-}4)$$

$$R_{g2} = \frac{2l_g}{\mu_0 A_e} \quad (22\text{-}5)$$

Where A_e was the cross-sectional area of the core center leg, l_1 and l_2 were the length and height of the core. The relation between the magnetizing inductance and the airgap was

$$L_m = \frac{\mu_0\mu_r A_e n_p^2}{(L_1+4L_2+3\mu_r l_g)} \quad (23)$$

From the above equation, a lower value of lg increased the L_m. The l_g could be arrived from the earlier equation as

$$l_g = \frac{\mu_0 A_e n_p^2}{3L_m} - \frac{l_1 + 4l_2}{3\mu_r} \tag{24}$$

ELP 64/10/50 from TDK with magnetic material N87 for the 3kW output power of the magnetic core was selected. Table 3 was used to design the magnetic core parameters of the high-frequency planar transformer of C2LC converter. l_g and l_b were calculated using Equations 21 & 24 for the corresponding optimized value of the leakage and magnetizing inductances.

Table 3 Magnetic core parameters of HFT

Parameter	Value	Parameter	Value	Parameter	Value
V_e	83000mm^3	A_e	1038mm^2	k_c	3.716 x10^{-24}
α	4.823	β	5.521	μ_r	1490
n_p, n_s	18	m_p, m_s	5	W_w	20mm
d_p, d_s,	80μm	d_i	0.2mm	W_d	102mm
l_1, l_2	62mm,10mm	l_g	0.17mm	l_b	8.34mm

4. Simulation and Experimental Results

A 3kW Off board EV charger for the specifications mentioned in the previous section was simulated in MATLAB for both manual design values and proposed TLBO+PSO optimized algorithm values. The simulation performance was validated by building a hardware setup with the optimized design values. During the process, the hardware setup of a bi-directional EV charger using a C2LC converter was shown in Figure 8(a). The boost converter-based power factor corrector (PFC) circuit converted the 230V AC input into 350V DC. Relating to the analysis, the results were obtained for the battery with a rating of 48V 60Ah. The results were obtained under 40% of State of charge of the battery. PWM method was used with PI controller parameters of Kp= 0.0499 and Ki= 0.00499 to control PFC circuit. The open loop C2LC converter switching pulses with 85kHz were generated using TMS320F28379D real-time digital signal processor controller. The waveforms of switching pulses of primary side switches Q_1/Q_3, Q_2/Q_4 were shown in Figure 8(b). The grid input voltage and current and the output voltage and current were shown in Figure 8(c) the analysis indicated that the distortion factor was very low in the current waveform, following the input voltage waveform to maintain a high power factor.

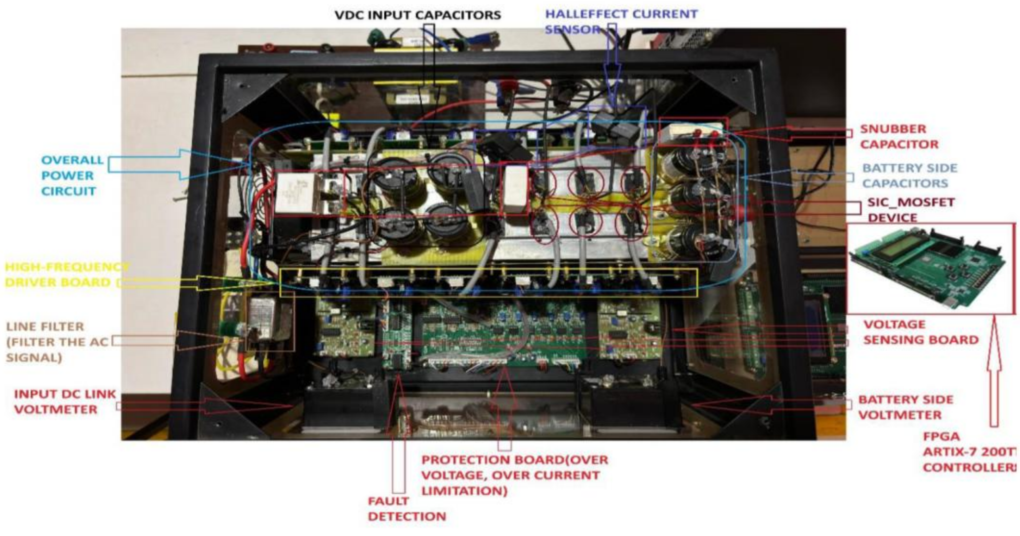

(a)

Figure 8(a) Hardware setup of EV charger (b) Switching pulse signals V_{g1} (Q_1, Q_4) V_{g2} (Q_2, Q_3) (c) Input AC and Output DC waveforms (d) Efficiency comparison of C2LC converter for manual and AI-optimized design parameters

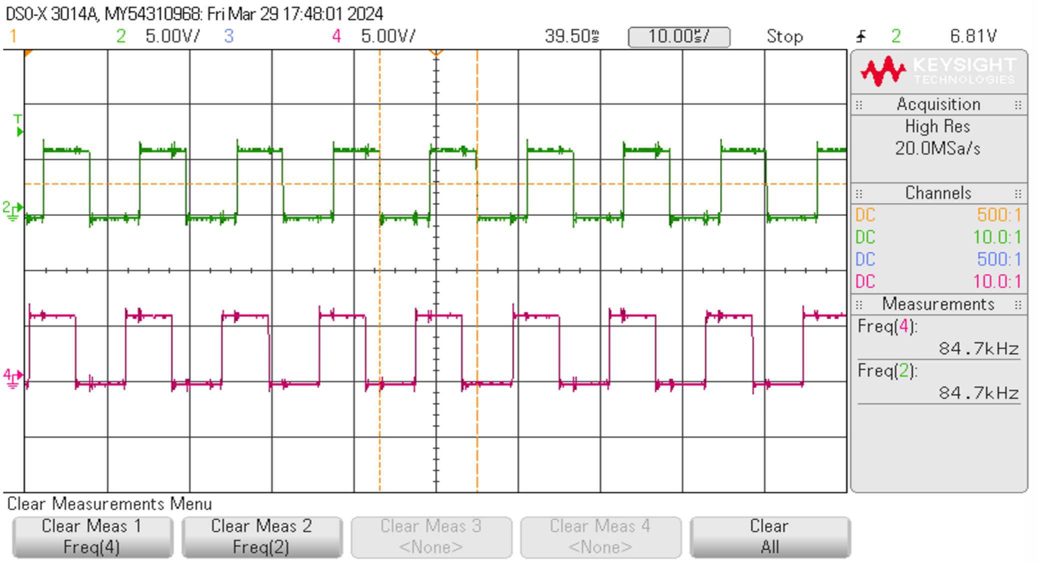

(b)

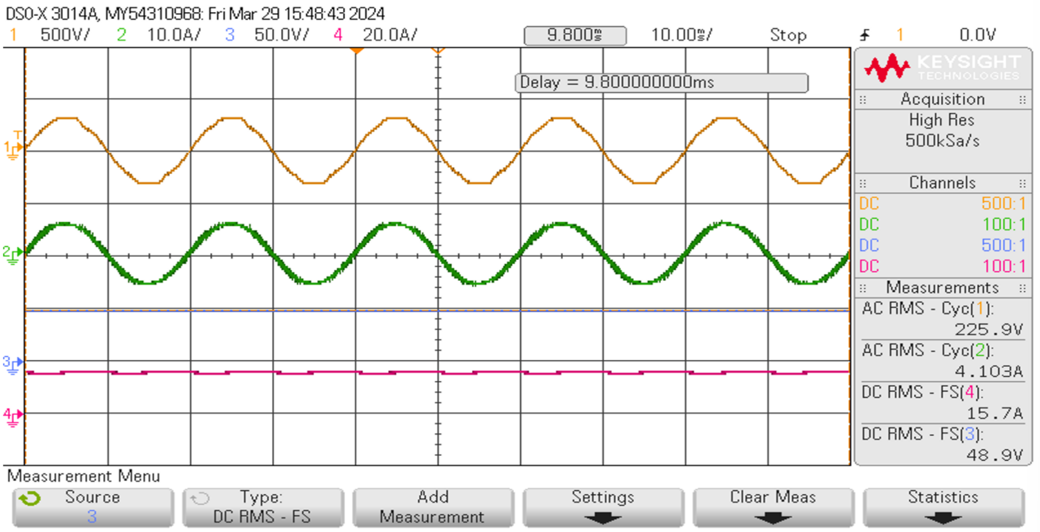

(c)

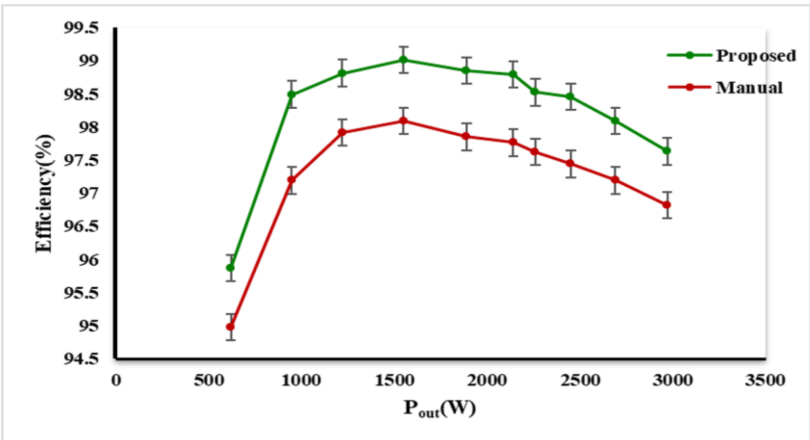

(d)

Figure 8(a) Hardware setup of EV charger (b) Switching pulse signals V_{g1} (Q_1, Q_4) V_{g2} (Q_2, Q_3) (c) Input AC and Output DC waveforms (d) Efficiency comparison of C2LC converter for manual and AI-optimized design parameters (Cont.)

The battery charging was achieved by Constant Current control to ensure better performance from the battery. Simulations for both manual calculation values and optimized values validated the AAIA-based optimal C2LC converter design. The efficiency was calculated for different output power values for both manual and optimized design values. Following the process of this study, the models were compared in Figure 8(d). The efficiency at the peak power with 0.98 power factor and THD of 2.3% was 96%. The constant voltage was maintained for the variation in the load and mains. The overall efficiency depended on DC-link voltage, which affected the stresses on the semiconductor switches. As the magnetic element losses were constant, the switch conduction and switching losses depended on DC-link voltage. The losses could be significantly reduced by replacing Si switches with SiC switches, respectively. ACM018P120QNN SiC MOSFET switches were used to minimize conduction loss to a great level. As the power level increased, the efficiency improved, and the low power substantially decreased the efficiency.

5. Conclusion

In conclusion, this study proposed the hybrid TLBO+PSO optimized C2LC converter design for achieving high efficiency for EV charging applications. The study focused on total power loss minimization and hybrid electromagnetic analysis to design the optimal HFT parameters. During the process, an EV charger was designed and implemented with these optimal design values. Due to this implementation, accuracy was increased, and the computational burden was significantly reduced. There was a considerable improvement in the converter performance due to this optimal design procedure. The hybrid electromagnetic analysis, design of airgap, as well as distance between the primary and secondary winding, majorly reduced the transformer loss. This EV charger using a C2LC converter dramatically influenced the efficiency of the charger performance with high power density. During the process, the experimental results validated the performance of this study.

Acknowledgements

The authors are grateful to Royal Academy of Engineering, Award reference No. TSP-2325-5-IN\172 for the support. This study was conducted at School of Electrical Engineering, Vellore Institute of Technology, and Vellore, India.

Author Contributions

Rajalakshmi M.: Conceptualization, Investigation, Methodology, Writing – original draft.
Razia Sultana W.: Investigation, Supervision, Validation, Writing – review & editing.

Conflict of Interest

The authors declare no conflicts of interest.

References

Ansari, SA, Davidson, JN & Foster, MP 2022, 'Fully-integrated planar transformer with a segmental shunt for LLC resonant converters', *IEEE Transactions on Industrial Electronics*, vol. 69, no. 9, pp. 9145–9154, https://doi.org/10.1109/TIE.2021.3116574

Attia, H & Suan, FTK 2024, 'Robust sliding mode controller design for boost converter applications', *International Journal of Technology*, vol. 15, no. 3, pp. 481–491, https://doi.org/10.14716/ijtech.v15i3.5164

Binay Kumar, Ritesh Kumar Singh, SK 2018, 'Genetic algorithm-based multi-criteria approach to product modularization', *International Journal of Technology*, vol. 4, no. 4, pp. 775–786, https://doi.org/10.14716/ijtech.v9i4.819

De Leon-Aldaco, SE, Calleja, H & Aguayo Alquicira, J 2015, 'Metaheuristic optimization methods applied to power converters: A review', *IEEE Transactions on Power Electronics*, vol. 30, no. 12, pp. 6791–6803, https://doi.org/10.1109/TPEL.2015.2397311

Dharma, IGSS & Setiawan, R 2024, 'Comparative review of multiobjective optimization algorithms for design and safety optimization in electric vehicles', *IEEE Access*, vol. 12, pp. 146376–146396, https://doi.org/10.1109/ACCESS.2024.3475032

Fathollahi, A, Gheisarnejad, M, Andresen, B, Farsizadeh, H, Khooban, M-H 2023, 'Robust artificial intelligence controller for stabilization of full-bridge converters feeding constant power loads', *IEEE Transactions on Circuits and Systems II: Express Briefs*, vol. 70, no. 9, pp. 3504–3508, https://doi.org/10.1109/TCSII.2023.3270751

Hajihosseini, M., Andalibi, M, Gheisarnejad, M, Farsizadeh, H & Khooban, M-H 2020, 'DC/DC power converter control-based deep machine learning techniques: Real-time implementation', *IEEE Transactions on Power Electronics*, vol. 35, no. 10, pp. 9971–9977, https://doi.org/10.1109/TPEL.2020.2977765

Hannan, MA, Faisal, M, Ker, PJ, Begum, RA, Dong, ZY, Zhang, C 2020, 'Review of optimal methods and algorithms for sizing energy storage systems to achieve decarbonization in microgrid applications', *Renewable and Sustainable Energy Reviews*, vol. 131, p. 110022, https://doi.org/10.1016/j.rser.2020.110022

Hasanah, RN, Yuniar, F, Setyawati, O, Suyono, H, Sawitri, DR & Taufik, T 2024, 'A modified perturb-and-observe control for improved maximum power point tracking performance on grid-connected photovoltaic system', *International Journal of Technology*, vol. 15, no. 1, pp. 99–109, https://doi.org/10.14716/ijtech.v15i1.5316

He, P & Khaligh, A 2017, 'Comprehensive analyses and comparison of 1 kW isolated DC-DC converters for bidirectional EV charging systems', *IEEE Transactions on Transportation Electrification*, vol. 3, no. 1, pp. 147–156, https://doi.org/10.1109/TTE.2016.2630927

Isen, E 2022, 'Determination of different types of controller parameters using metaheuristic optimization algorithms for buck converter systems', *IEEE Access*, vol. 10, pp. 127984–127995, https://doi.org/10.1109/ACCESS.2022.3227347

Jamahori, HN, Abdullah, MP, Ali, A, AlKassem, A 2024, 'Optimal design and performance analysis of multiple photovoltaic with grid-connected commercial load', *International Journal of Technology*, vol. 15, no. 4, pp. 834–846, https://doi.org/10.14716/ijtech.v15i4.6019

Jamahori, HN, Abdullah, MP, Ali, A, AlKassem, A 2024, 'Optimal design and performance analysis of multiple photovoltaic with grid-connected commercial load', *International Journal of Technology*, vol. 15, no. 4, pp. 834–846, https://doi.org/10.14716/ijtech.v15i4.6019

Jamahori, HN, Abdullah, MP, Ali, A, AlKassem, A 2024, 'Optimal design and performance analysis of multiple photovoltaic with grid-connected commercial load', *International Journal of Technology*, vol. 15, no. 4, pp. 834–846, https://doi.org/10.14716/ijtech.v15i4.6019

Jayalath, S & Khan, A 2021, 'Design, challenges, and trends of inductive power transfer couplers for electric vehicles: A review', *IEEE Journal of Emerging and Selected Topics in Power Electronics*, vol. 9, no. 5, pp. 6196–6218, https://doi.org/10.1109/JESTPE.2020.3042625

Jayawardana, A, Ashish PA, Duane AR, Fiorentini & Massimo 2019, 'Optimisation framework for the operation of battery storage within solar-rich microgrids', *IET Smart Grid*, vol. 2, no. 4, pp. 504–513, https://doi.org/10.1049/iet-stg.2019.0084

Khorashadizade, M & Hosseini, S 2023, 'An intelligent feature selection method using binary teaching-learning based optimization algorithm and ANN', *Chemometrics and Intelligent Laboratory Systems*, vol. 240, p. 104880, https://doi.org/10.1016/j.chemolab.2023.104880

Lee, FC, Li, Q & Nabih, A 2021, 'High frequency resonant converters: an overview on the magnetic design and control methods', *IEEE Journal of Emerging and Selected Topics in Power Electronics*, vol. 9, no. 1, pp. 11–23, https://doi.org/10.1109/JESTPE.2020.3011166

Lee, W-S, Kim, J-H, Lee, J-Y & Lee, I-O 2019, 'Design of an isolated DC/DC topology with high efficiency of over 97% for ev fast chargers', *IEEE Transactions on Vehicular Technology*, vol. 68, no. 12, pp. 11725–11737, https://doi.org/10.1109/TVT.2019.2949080

Li, X, Huang, J, Ma, Y, Wang, X, Yang J & Wu, X 2022, 'Unified modeling, analysis, and design of isolated bidirectional CLLC resonant DC-DC converters', *IEEE Journal of Emerging and Selected Topics in Power Electronics*, vol. 10, no. 2, pp. 2305–2318, https://doi.org/10.1109/JESTPE.2022.3145817

Li, X, Zhang, X, Lin, F, Sun, C, Mao, K 2023, 'Artificial-intelligence-based hybrid extended phase shift modulation for the dual active bridge converter with full zvs range and optimal efficiency', *IEEE Journal of Emerging and Selected Topics in Power Electronics*, vol. 11, no. 6, pp. 5569–5581, https://doi.org/10.1109/JESTPE.2022.3185090

Li, Z, Hsieh, E, Li, Q, Lee, FC 2023 'High-frequency transformer design with medium-voltage insulation for resonant converter in solid-state transformer', *IEEE Transactions on Power Electronics*, vol. 38, no. 8, pp. 9917–9932, https://doi.org/10.1109/TPEL.2023.3279030

Lin, F, Zhang, X, Li, X, Sun, C, Zsurzsan, G, Cai, W, Wang, C 2024, 'AI-based design with data trimming for hybrid phase shift modulation for minimum-current-stress dual active bridge converter', *IEEE Journal of Emerging and Selected Topics in Power Electronics*, vol. 12, no. 2, pp. 2268–2280, https://doi.org/10.1109/JESTPE.2022.3232534

Liu, H, Cui, S, Zhang, H, Hu, Y, Xue, Y & Liu, C 2022, 'Hybrid bidirectional DC/DC converter: Mutual control and stability analysis', *CSEE Journal of Power and Energy Systems [Preprint]*, https://doi.org/10.17775/cseejpes.2021.00260

Mao, L-L, Zain, AM, Zhou, KQ, Qin, Feng, W, Fang, L 2024 'A systematic review of wind driven optimization algorithms and their variants', *IEEE Access*, vol. 12, pp. 120023–120063, https://doi.org/10.1109/ACCESS.2024.3449998

Martins, LF, Stone, D & Foster, M 2019, 'Modelling of bidirectional CLLC resonant converter operating under frequency modulation', *2019 IEEE Energy Conversion Congress and Exposition, ECCE 2019*, pp. 3750–3757, https://doi.org/10.1109/ECCE.2019.8913203

Mirtchev, A & Tatakis, E 2022, 'Design methodology based on dual control of a resonant dual active bridge converter for electric vehicle battery charging', *IEEE Transactions on Vehicular Technology*, vol. 71, no. 3, pp. 2691–2705, https://doi.org/10.1109/TVT.2022.3142681

Mukherjee, S & Barbosa, P 2023, 'Design and optimization of an integrated resonant inductor with high-frequency transformer for wide gain range DC-DC resonant converters in electric vehicle charging applications', *IEEE Transactions on Power Electronics*, vol. 38, no. 5, pp. 6380–6394, https://doi.org/10.1109/TPEL.2023.3243807

Nagesha, C & Lakshminarasamma, N 2023, 'High-gain bidirectional lclc resonant converter with reconfigureurable capability', *IEEE Transactions on Power Electronics*, vol. 38, no. 2, pp. 1871–1886, https://doi.org/10.1109/TPEL.2022.3211205

Priyadarshi, N, Padmanaban, S, Maroti, KP & Sharma, A 2019, 'An extensive practical investigation of fpso-based mppt for grid integrated pv system under variable operating conditions with anti-islanding protection', *IEEE Systems Journal*, vol. 13, no. 2, pp. 1861–1871, https://doi.org/10.1109/JSYST.2018.2817584

Rahman, I, Vasant, PM, Singh, BSM, Abdullah-al-wadud, M & Adnan, N 2016, 'Review of recent trends in optimization techniques for plug-in hybrid , and electric vehicle charging infrastructures', *Renewable and Sustainable Energy Reviews*, vol. 58, pp. 1039–1047, https://doi.org/10.1016/j.rser.2015.12.353

Rajalakshmi, M & Sultana, WR 2022, 'Comparison of wireless charging compensation topologies of electric vehicle', *Smart Grids and Green Energy System*, pp. 285–300

Rajalakshmi, M & Sultana, WR 2024, 'Model predictive controller-based Convolutional Neural Network controller for optimal frequency tracking of resonant converter-based EV charger', *Results in Engineering*, vol. 24 (December), p. 103658, https://doi.org/10.1016/j.rineng.2024.103658

Rajalakshmi, M, & Sultana, WR 2023, 'Bidirectional wireless charging for vehicle to grid and vehicle to vehicle applications', *2023 Innovations in Power and Advanced Computing Technologies (i-PACT), IEEE*, pp. 1–6, https://doi.org/10.1109/i-PACT58649.2023.10434433

Rajalakshmi, M, Prashant, KS, Sivagnanam, G, Bhartia, A, Sultana, WR & Chitra, A 2021, 'Design and analysis of multi-input cllc converter for charging application', *3rd IEEE International Virtual Conference on Innovations in Power and Advanced Computing Technologies, i-PACT 2021*, pp. 1–7, https://doi.org/10.1109/i-PACT52855.2021.9696719

Shalbaf, AA, Shahidi, N & Hemati, M 2024, 'A high-gain interleaved DC-DC converter with reduced components for EV charging application', *Computers and Electrical Engineering*, vol. 118(PA), p. 109316, https://doi.org/10.1016/j.compeleceng.2024.109316

Silva, FLd, Glatt, R, Su, W, Bui, V-H, Chang, F, Chaturvedi, S, Wang, M, Murphey, YL, Huang, C, Xue, L & Zeng, R 2023, 'AutoTG: Reinforcement learning-based symbolic optimization for AI-assisted power converter design', *IEEE Journal of Emerging and Selected Topics in Industrial Electronics*, vol. 5, no. 2, pp. 680–689, https://doi.org/10.1109/jestie.2023.3303836

Song, J, Dong, F, Zhao, J, Wang, H, He, Z & Wang, L 2019, 'An efficient multiobjective design optimization method for a pmslm based on an extreme learning machine', *IEEE Transactions on Industrial Electronics*, vol. 66, no. 2, pp. 1001–1011, https://doi.org/10.1109/TIE.2018.2835413

Yashin, S, Yashina, N, Koshelev, E, Kashina, O & Pronchatova-Rubtsova, N 2020, 'Foresight of volga federal district innovation system development using a multi-objective genetic algorithm', *International Journal of Technology,* vol. 11, no. 6, pp. 1171–1180, https://doi.org/10.14716/ijtech.v11i6.4432

Zhou, G, Zhou, Y, Deng, W, Yin, S & Zhang, Y 2023, 'Advances in teaching–learning-based optimization algorithm: A comprehensive survey (ICIC2022)', *Neurocomputing*, vol. 56, p. 126898, https://doi.org/10.1016/j.neucom.2023.126898

Zhou, M, Shu, D & Wang, H 2022, 'An H5-bridge-based laddered CLLC DCX with variable DC link for PEV charging applications', *IEEE Transactions on Power Electronics*, vol. 37, no. 4, pp. 4249–4260, https://doi.org/10.1109/TPEL.2021.3123179